JMEPEG (2023) 32:4768–4776
https://doi.org/10.1007/s11665-022-07430-y

1059-9495/$19.00

TECHNICAL ARTICLE

Stress Softening Behavior and Microstructural Characterization of Al-Zn-Mg-Sc Alloy with High Zn Concentration Subjected to Isothermal Compression

Hengxing Wang, Fangcheng Qin, Chongyu Liu, and Yangbo Wang

Submitted: 21 April 2022 / Revised: 28 August 2022 / Accepted: 4 September 2022 / Published online: 28 September 2022

The isothermal compression tests were conducted to study the hot compression behavior of Al-Zn-Mg-Sc alloy with high Zn concentration using a Gleeble-3500 thermal simulator in the temperature range of 300-450 °C and strain rate range of 0.01-5 s^{-1}. The stress softening behavior was analyzed, and the constitutive model was established to describe the hot compression behavior of the high Zn alloy. The microstructure evolution mechanism was clarified by optical microscopy and electron backscatter diffraction. The results indicate that the true stress rapidly increases to the peak value with the increasing accumulative true strain, and finally reaches to a steady state. As the strain rate increases and temperature decreases, the peak stress increases, and the isothermal compression behavior is regarded as a competing process of work hardening and flow softening. The softening mechanism is highly affected by the compression temperature and strain rate. The Al-Zn-Mg-Sc alloy with high Zn is characterized by the dynamic recovery at the low temperature and high strain rate. And both the dynamic recovery and dynamic recrystallization dominate at the high temperature and low strain rate. The relatively stronger ⟨111⟩ orientation plays a key role in developing the recrystallization grains. As the compression temperature increases and strain rate decreases, many sub-grains with low-angle grain boundaries are transformed into recrystallized grains with high-angle grain boundaries. The main softening mechanism is also transformed from dynamic recovery to dynamic recrystallization.

Keywords Al-Zn-Mg-Sc alloy, constitutive model, hot compression behavior, microstructure evolution, misorientation distribution

1. Introduction

Due to the characteristics of dynamic precipitation, excellent damping and mechanical properties, the Al-Zn alloy components with high Zn concentration approximately 15-40% as the data storage devices, such as hard disk box body have been widely used in the exploration of deep space and ocean applications (Ref 1, 2). The Mg element added to the Al-(15 ∼ 40)Zn alloys can react with Zn to precipitate η', η and Zn phase, resulting in a considerable improvement of mechanical properties by precipitation strengthening effect (Ref 3-6). In addition, the Al_3Sc particles were precipitated by adding Sc element into the Al-(15 ∼ 40)Zn alloys. The refined grains with high-angle grain boundaries were caused by the pinning effect of Al_3Sc particles during hot deformation process (Ref 7-9). Meanwhile, the mechanical properties of Al-15Zn alloys, Al-20Zn alloys, Al-35Zn alloys are considerably improved by means of the hot working such as hot rolling, high pressure torsion, equal channel angular extrusion, etc., (Ref 6, 8, 10). For example, the ductility of Al-30Zn alloys also enhanced due to grain refinement in high pressure torsion (Ref 11). The hardness of Al-Zn-Mg alloy increased by 67 and 104% after applying the first and second equal channel angular extrusion, respectively (Ref 12). The η' and Zn phase are induced and the high yield strength of 436 MPa and elongation of 5.2% are obtained by extruding Al-27Zn-1.5 Mg alloys (Ref 13). In addition, the grains are refined by adding 0.3% Sc into the Al-Zn-Mg alloys during extrusion, and the resultant strength and elongation enhanced with the increases in Sc content (Ref 14).

The study of the hot compression behavior of the Al-Zn alloys with high Zn concentration is essential to optimize processing parameters. The microstructure evolution and the resultant mechanical properties of the Al-Zn alloys are highly affected by compression temperature and strain rate. For the hot compression of the Al-Zn alloys, the main softening mechanism of microstructure is characterized by dynamic recovery (DRV) and dynamic recrystallization (DRX) (Ref 15, 16). The DRV is a softening process featured by the thermal activation, dislocation cancellation and rearrangement during hot compression of metals and alloys. And the DRX is the main softening mechanism of commercial aluminum alloys (Ref 17). Meanwhile, the DRX is characterized by the dislocations aggregation, which causes the formation of low-angle grain boundaries under the high dislocation density (Ref 18-20). As the dislocation density in the sub-grains increases, the low-angle grain boundaries transforms into high-angle grain boundaries by absorbing dislocations (Ref 21, 22). Moreover, the hot compression behavior of aluminum alloys is reflected

Hengxing Wang, Fangcheng Qin, Chongyu Liu, and **Yangbo Wang**, College of Materials Science and Engineering, Guilin University of Technology, Guilin, China. Contact e-mail: qinfangcheng@glut.edu.cn.

by flow stress, which is related to the true strain, strain rate, and temperature (Ref 23). As with microstructure characterization, the constitutive model is also widely used to describe the hot compression behavior of alloys under specific conditions (Ref 24-27). In last decades, it is reported that the relationship among temperature, strain rate and strain can be accurately represented by the Arrhenius-type constitutive model (Ref 28-31). However, the study on the softening behavior and constitutive model of Al-Zn alloys with the addition of Sc and Mg element subjected to hot compression deformation is rarely seen (Ref 6-9, 32-34). Thus, in this study, the isothermal compression tests were used to study the hot compression behavior and microstructure evolution of a cast Al-Zn-Mg-Sc alloy with high Zn concentration, and the constitutive model was established. The stress softening behavior and microstructure evolution mechanism were clarified by characterizing grain orientation, grain size and misorientation distribution. The studied cast alloy will be used to produce the hard disk box body by extrusion technique. Compared with a wrought alloy, the direct extrusion of a cast alloy has prominent advantages such as shortening process, saving materials and energy, reducing equipment investment, etc. Finally, these results will provide the theoretical basis and experimental guidance for the future extrusion forming of the Al-Zn-Mg-Sc alloy hard disk box body.

2. Materials and Experimental Methods

The Al-20Zn-0.5Mg-0.5Sc alloy ingots with a thickness of 40 mm, a length of 150 mm and a width of 100 mm were prepared by melting pure Al (4 N), pure Zn (4 N), Al-10Mg and Al-2Sc master alloys in a resistance heating furnace with a graphite crucible. According to the detection of direct reading spectrometry, the actual chemical compositions of the alloy ingot was 20 Zn, 0.5 Mg, 0.5 Sc, and Bal. Al (wt.%). The melting and pouring temperatures were 700 °C, and the casting mold was graphite. The alloy ingot was homogenized at 470 °C × 12 h in a resistance furnace. For isothermal compression tests, the cylinder specimens with 10 mm in diameter and 15 mm in height were machined from the homogenized ingot. The Gleeble-3500 thermal simulator was used to conduct the tests (Ref 35). To reduce the effect of friction on the compression behavior, the graphite lubricant was applied in the interface of the anvils and the specimen (Ref 36). Before compression, the specimens were respectively heated to 300, 350, 400, and 450 °C at a heating rate of 5 °C/s, and then held for 120 s to obtain a uniform temperature distribution. The 0.01, 0.1, 1 and 5 s^{-1} were selected as the strain rates in this compression. The final true strain of approximately 0.9 was achieved. After compression, the specimens were immediately cooled in water to room temperature for preserving the deformed microstructure (Ref 35). Subsequently, all compressed specimens were subjected to solid solution at 470 °C and soaked for 1 h, and aging at 120 °C and held for 17 h. The hot compressed specimens were cut along the compression axis. Half of the specimens were etched in Keller mixed acid solution (2.5 mL HNO_3 + 1.5 mL HCI + 1 mL HF + 95 mL H_2O) after mechanically grounded and polished according to the standard methods. The microstructures of the corroded specimens were observed by metallographic microscope (LEICA-DMI8A). The other half of the specimens were electro polished (voltage 12 V, current 1.0 A, time 10 s) in mixed acid solution (10%$HClO_4$ + 90%C_2H_5OH). Electron backscattering diffraction (EBSD) pattern analysis with a step size of 1 μm was performed using a field emission scanning electron microscope (ZEISS ULTRA-55). The grain size, grain orientation, misorientation distribution and recrystallization degree of the tested specimens were characterized using HKL Channel 5 software.

3. Results and Discussion

3.1 Stress Softening Behavior

The true stress–strain curves recorded from the isothermal compression tests are widely used to describe the hot compression behavior among true stress, strain rate, temperature, and true strain. The true stress–strain curves of the Al-Zn-Mg-Sc alloy with high Zn concentration obtained by hot compression at different conditions are shown in Fig. 1. From the curves, the true stress decreases with increasing compression temperature and decreasing strain rate. In the early stage of hot compression, the true stress increases sharply with increasing accumulative true strain, and then reaches a peak true stress value due to work hardening (WH). Due to flow softening, the true stress decreases to a steady state after the peak value with increasing accumulative strain. During the isothermal compression of the Al-Zn-Mg-Sc alloy, the competing mechanism between work hardening and flow softening produce a crucial effect on the true stress. Thus, the true stress–strain curves of the Al-Zn-Mg-Sc alloy with high Zn concentration are divided into two stages. In the first stage, there are a lot of defects in this alloy, which cause the movement of dislocations to be hindered. In this stage, the hardening rate is significantly greater than the softening rate, especially at the higher strain rates of 1 s^{-1} and 5 s^{-1}. As shown in Fig. 1(c) and (d), the WH dominates and the peak true stress value increases rapidly. The peak value of true stress is approximately 100 MPa at 300 °C/5 s^{-1}, which is higher than 65 MPa at 300 °C/0.01 s^{-1}. In the second stage, the flow softening rate increases due to the DRV and DRX. It is widely reported that the DRV and DRX are the main flow softening form of aluminum alloys. The WH and flow softening reach an equilibrium state, which leads to the true stress–strain curves are almost flat and the true stress value no longer increases. For example, at the steady state of isothermal compression, the true stress values are 18 MPa at 450 °C/0.01 s^{-1} and 24 MPa at 400 °C/0.01 s^{-1}, respectively, which are lower than 45 MPa at 450 °C/1 s^{-1} and 60 MPa at 400 °C/1 s^{-1}. Thus, the stress softening behavior of the high Zn alloy is affected by the combination of WH, DRV and DRX under different compression temperature and strain rate.

3.2 Constitutive Model

According to the above analysis of the curves, the change of the true stress of the high Zn alloy is closely related to the applied strain rate and compression temperature during isothermal compression, which is controlled by the thermal activation energy. It is reported that the relationship among the variables under different compression conditions is widely characterized by the following constitutive equation (Ref 35, 37):

$$\dot{\varepsilon} = f(\sigma)\exp[Q/RT] \quad \text{(Eq 1)}$$

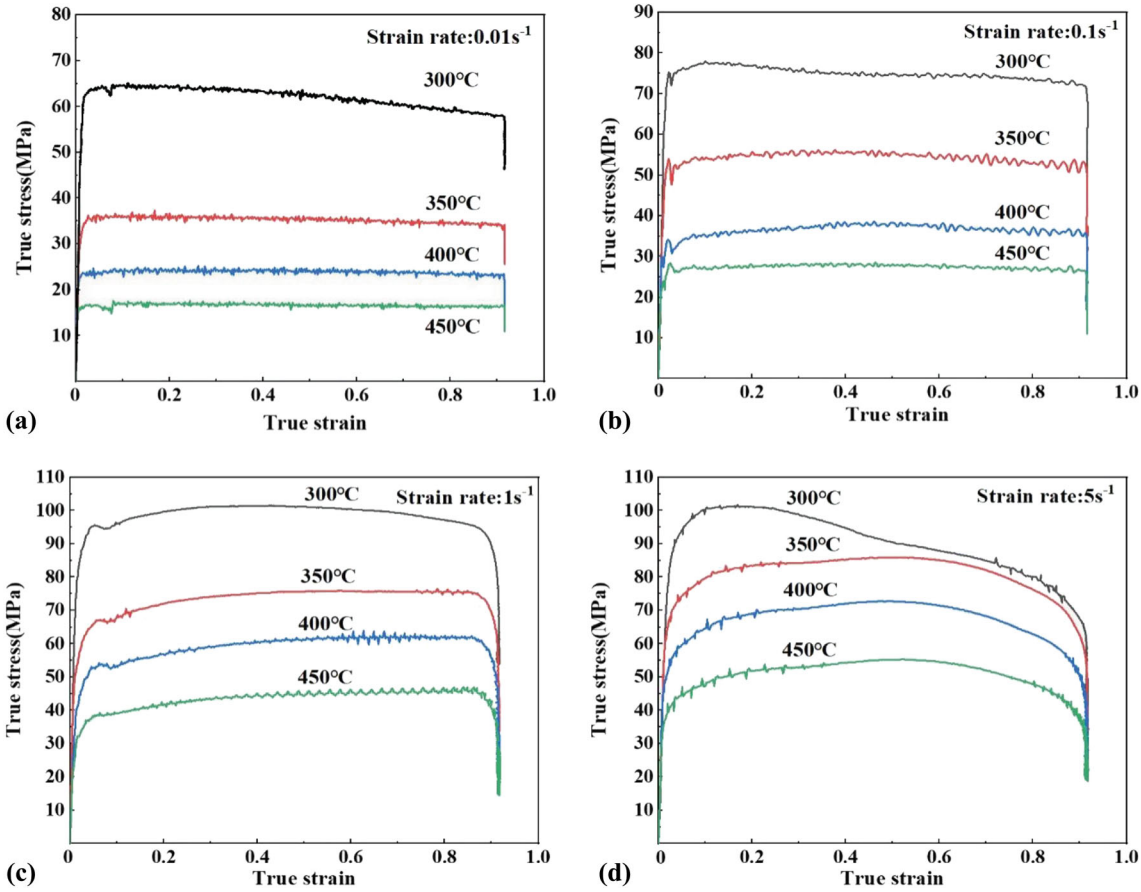

Fig. 1 True stress–strain curves of Al-Zn-Mg-Sc alloy with high Zn concentration under different strain rates: (a) 0.01 s^{-1}; (b) 0.1 s^{-1}; (c) 1 s^{-1}; and (d) 5 $s.^{-1}$

in which, $\dot{\varepsilon}$, σ, Q, R and T are the strain rate (s^{-1}), true stress (MPa), activation energy ($kJ{\cdot}mol^{-1}$), gas constant (8.314 $J{\cdot}mol^{-1}{\cdot}K^{-1}$) and absolute temperature (K), respectively.

The following Eq 2 is used for a wide range of true stress, and the relationship of $\dot{\varepsilon}$, T and σ is expressed as (Ref 35, 38):

$$f(\sigma) = [\sinh(\alpha\sigma)]^n \quad \text{(Eq 2)}$$

$$\dot{\varepsilon} = A[\sinh(\alpha\sigma)]^n \exp[-Q/RT] \quad \text{(Eq 3)}$$

At a constant compression temperature, Fig. 2(a)–(c) depicts the relationship of $\ln\dot{\varepsilon} - \ln\sigma$, $\ln\dot{\varepsilon} - \sigma$ and $\ln\dot{\varepsilon} - \ln[\sinh(\alpha\sigma)]$, respectively. The corresponding material constants are calculated as (Ref 39): $n_1 = 7.8735$, $\beta = 0.1404$, $n = 5.6505$, $\alpha = \beta/n_1 = 0.01783$. The slope of $\ln[\sinh(\alpha\sigma)] - (1/T)$ (depicts in Fig. 2d) is given as $S = 2.1852$.

By partial differentiation of Eq (1) (Ref 30), the value of Q is calculated as 102.657 $kJ{\cdot}mol^{-1}$. In addition, the Zener-Hollomon ($Z = \dot{\varepsilon}\exp[Q/RT]$) parameter is used to verify the relationship between strain rate and compression temperature, which is expressed as $Z = A[\sinh(\alpha\sigma)]^n$ (Ref 35, 40). The logarithm can be conducted to obtain the constant A.

The calculated values of $\ln Z$ are listed in Table 1. The intercept of $\ln Z - \ln[\sinh(\alpha\sigma)]$ (depicts in Fig. 2e) is calculated as $\ln A = 15.6356$, and the value of A is given as 6.17×10^6. Table 2 lists the values of material constants used in the constitutive model. Thus, the constitutive model for describing the hot compression behavior of Al-Zn-Mg-Sc alloy with high Zn concentration is established as follows:

$$\dot{\varepsilon} = 6.17 \times 10^6[\sinh(0.01783\sigma)]^{5.6505}\exp[\frac{-102.657}{RT}]. \quad \text{(Eq 4)}$$

3.3 Microstructural Characterization

Figure 3 shows the microstructures of the Al-Zn-Mg-Sc alloy after hot compressed at different compression temperatures with the strain rate of 0.1 s^{-1}. It can be seen from Fig. 3(a) and (b), the grains are elongated along the direction perpendicular to the compression axial after compressed at 300 and 350 °C, and the deformed microstructure is still preserved. Compared to the grains at 300 °C, the width of elongated grains increases when the temperature increasing to 350 °C. From Fig. 3(c), it can be found that the grain boundaries are jagged and some small equiaxed grains appear at the compression temperature of 400 °C. The appearance of refined grains is attributed to the DRX. Moreover, as the temperature increases to 450 °C, the number of fine equiaxed grains increases. And the size of recrystallized grains also increases, as shown in Fig. 3(d). Due to the DRX, the average sizes of grains are refined from 27 μm at 300 °C and 26.7 μm at 350 °C to approximately 10 μm at 400 °C and 8.6 μm at 450 °C. Meanwhile, the relatively homogeneous distributions of refined

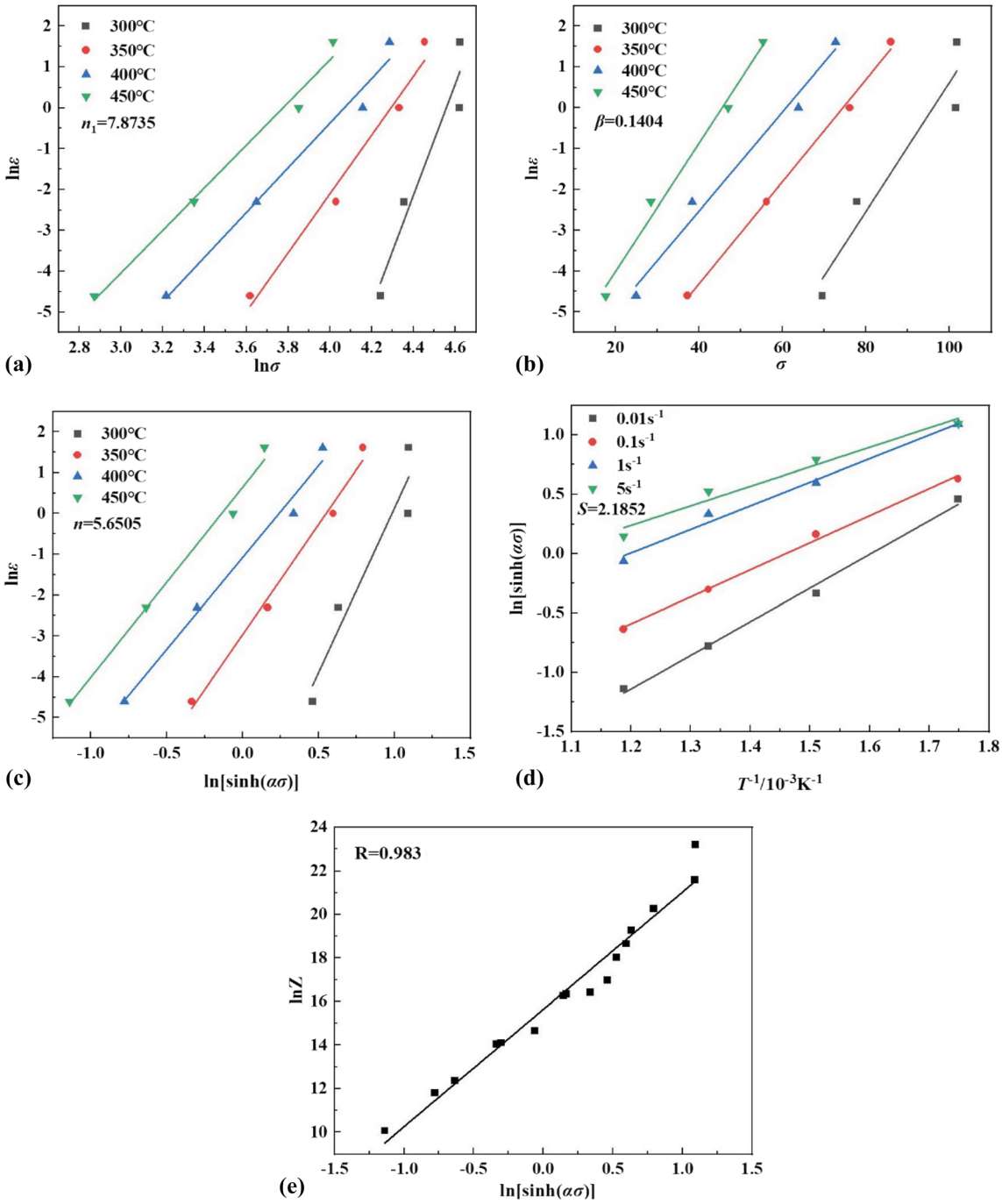

Fig. 2 Correlation between (a) $\ln\underline{\varepsilon} - \ln\sigma$; (b) $\ln\underline{\varepsilon} - \sigma$; (c) $\ln\underline{\varepsilon} - \ln[\sinh(\alpha\sigma)]$; (d) $\ln[\sinh(\alpha\sigma)] - (1/T)$; (e) $\ln Z - \ln[\sinh(\alpha\sigma)]$

Table 1 ln*Z* values of the Al-Zn-Mg-Sc alloy under isothermal compression

	Temperature, °C			
Strain rate, s^{-1}	300	350	400	450
0.01	16.98134	14.04662	11.81436	10.0593
0.1	19.28393	16.34921	14.11694	12.36189
1	21.58651	18.65179	16.41953	14.66447
5	23.19595	20.26123	18.02897	16.27391

Table 2 Values of material constants of the Al-Zn-Mg-Sc alloy under isothermal compression

α, MPa^{-1}	*n*	*Q*, kJ mol^{-1}	*A*, s^{-1}
0.01783	5.6505	102.657	6.17×10^6

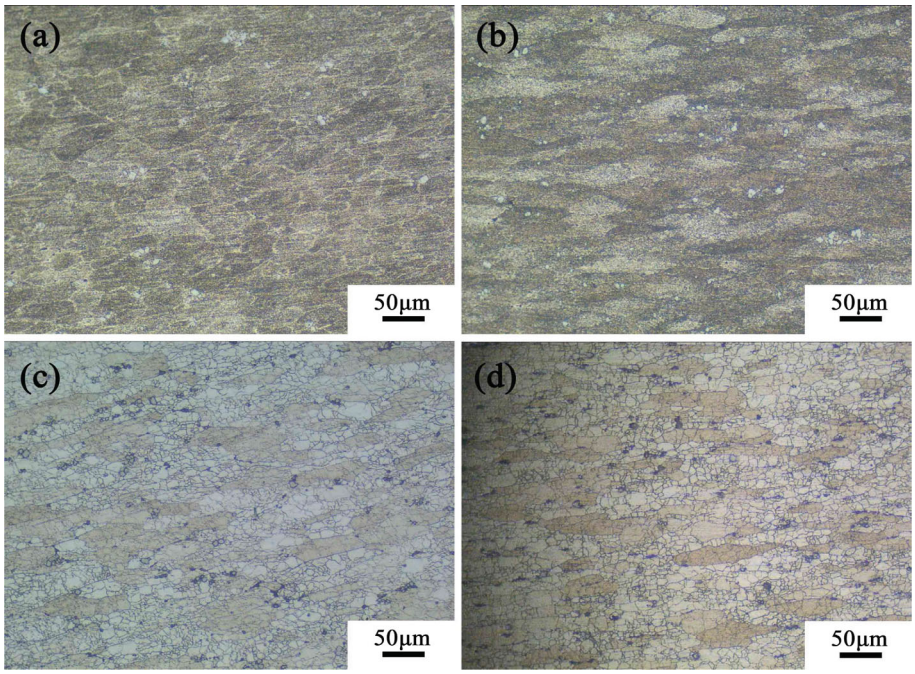

Fig. 3 Microstructures at different compression temperatures with the strain rate of 0.1 s^{-1}: (a) 300 °C; (b) 350 °C; (c) 400 °C; (d) 450 °C

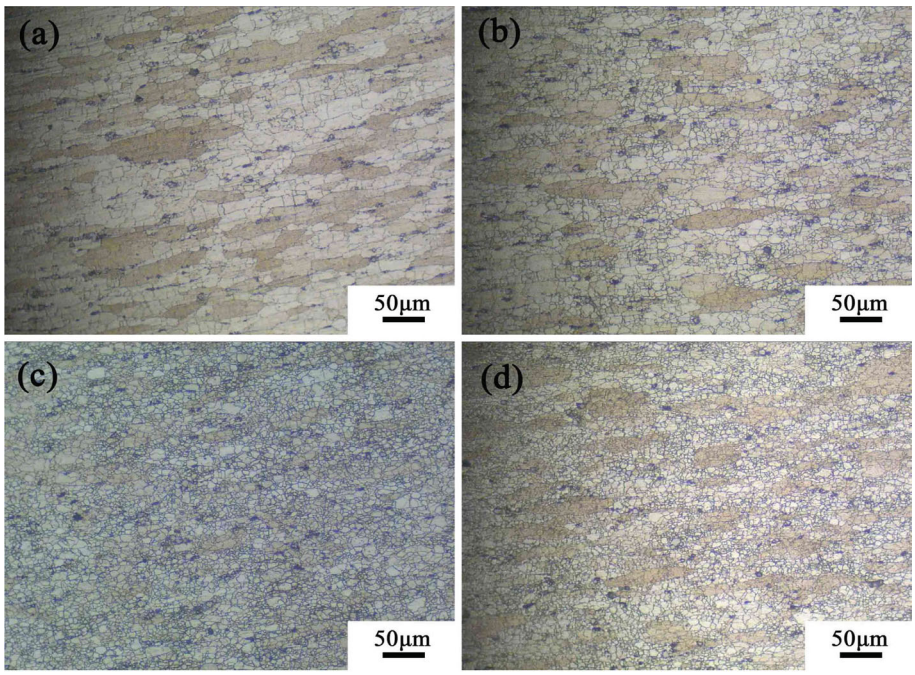

Fig. 4 Microstructures at different strain rates with the compression temperature of 450 °C: (a) 0.01 s^{-1}; (b) 0.1 s^{-1}; (c) 1 s^{-1}; (d) 5 s^{-1}

grains at the compression conditions of 400 °C/0.1 s^{-1} and 450 °C/0.1 s^{-1} are achieved.

Figure 4 presents the microstructures of the Al-Zn-Mg-Sc alloy after hot compressed at different strain rates with the compression temperature of 450 °C. Under different compression conditions, the elongated grains along the direction perpendicular to the compression axial are caused. At the strain rates of 0.01 s^{-1} and 0.1 s^{-1}, the large grain size and relatively uniform distribution are found. In Fig. 4(a) and (b), a small amount of second phase is precipitated at the grain boundaries. As the strain rate increases to 1 and 5 s^{-1}, the elongated and coarse grains are refined and the precipitation of the second phase at the grain boundaries are also enhanced, as shown in Fig. 4(c) and (d). It can be found that, the average sizes of grains are refined from 10.5 μm at 450 °C/0.01 s^{-1} to approximately 8.6 μm at 450 °C/0.1 s^{-1}, 6.2 μm at 450 °C/1 s^{-1} and 6 μm at 450 °C/5 s^{-1}, respectively. It mainly attributed to that the growth of grains is suppressed at the high strain rates. These results of microstructural characteristics affected by the

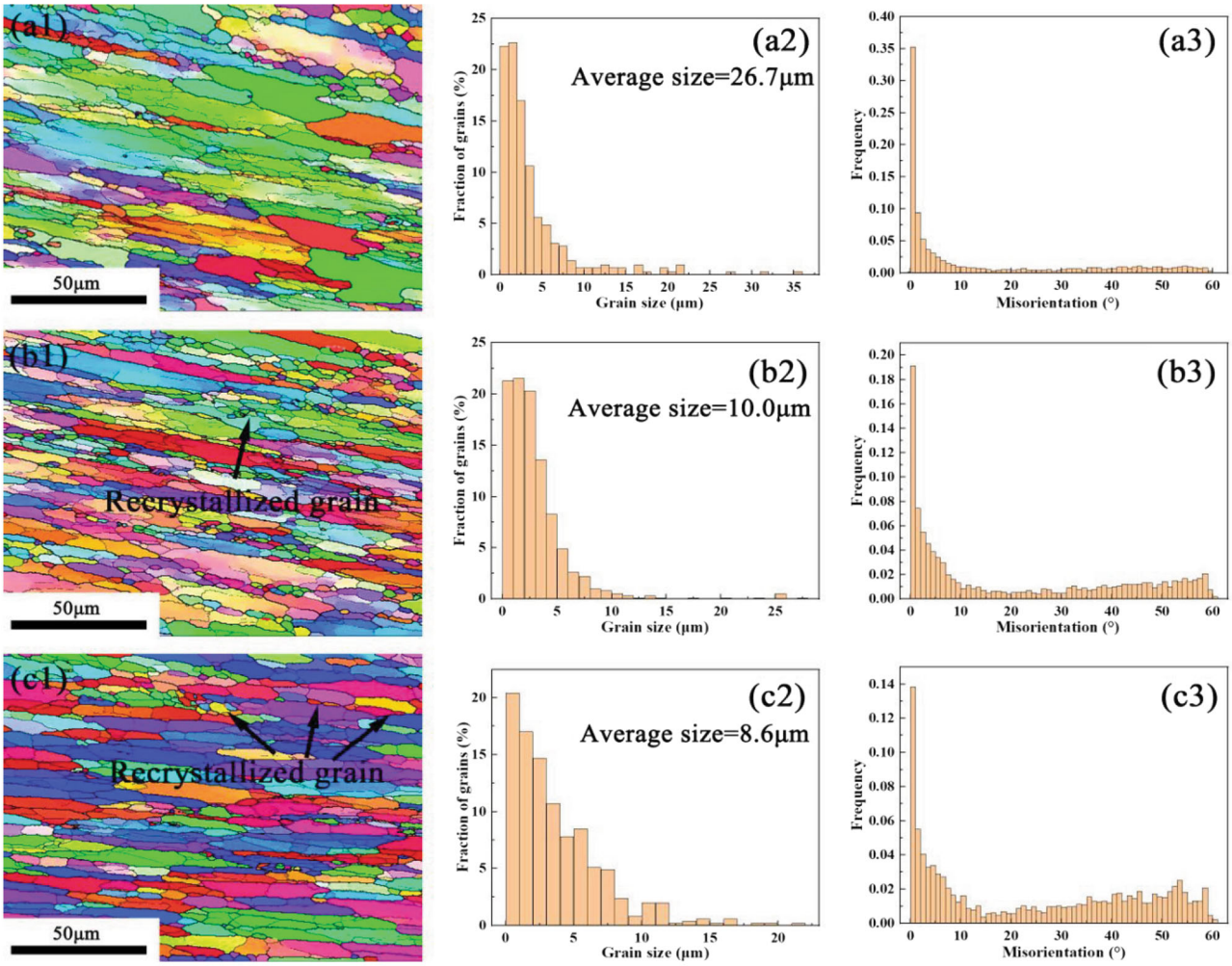

Fig. 5 EBSD IPF images, grain size and misorientation after hot compressed at different compression temperatures: (a1–a3) 350 °C; (b1–b3) 400 °C; (c1–c3) 450 °C

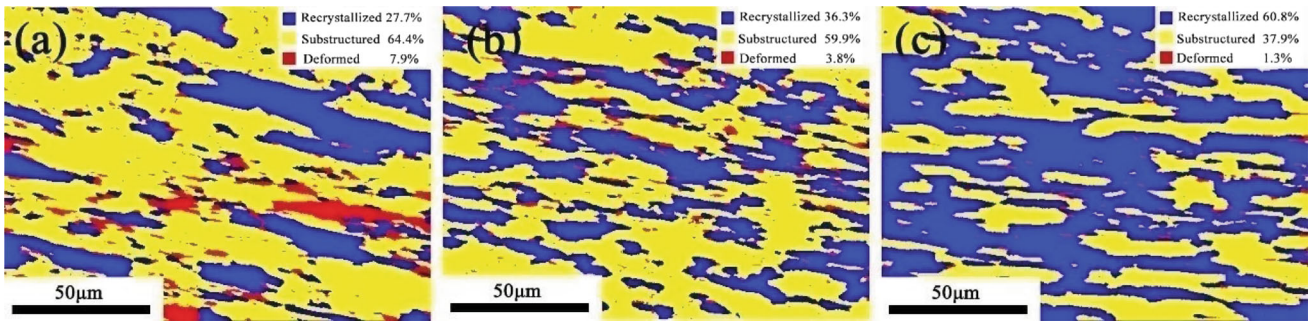

Fig. 6 The degree of recrystallization after hot compressed at different compression temperatures: (a) 350 °C; (b) 400 °C; (c) 450 °C

compression conditions are almost consistent with the reported literatures.

3.4 Softening Mechanism

To further determine the softening mechanism of the Al-Zn-Mg-Sc alloy with high Zn concentration in isothermal compression, the EBSD images are presented in Fig. 5 and 6. The hot compression behavior can be clarified using the inverse pole figures (IPF) by evaluating the grain orientation. Figure 5 shows the grain orientation, grain size and misorientation distribution of the alloy at different compression temperatures with the strain rate of 0.1 s^{-1}. Two types of grains can be found from the EBSD images: the elongated thin strip-like grains, and the fine equiaxed grains with a chain-like structure distributed along the boundaries of coarse grains. It can be seen from Fig. 5(a1)–(a3), the elongated grains dominate at the temperature of 350 °C, and the sub-grains with different sizes and irregular shapes appear, implying a DRV mechanism. Figure 5(b1)–(b3) presents that the fine equiaxed recrystallized

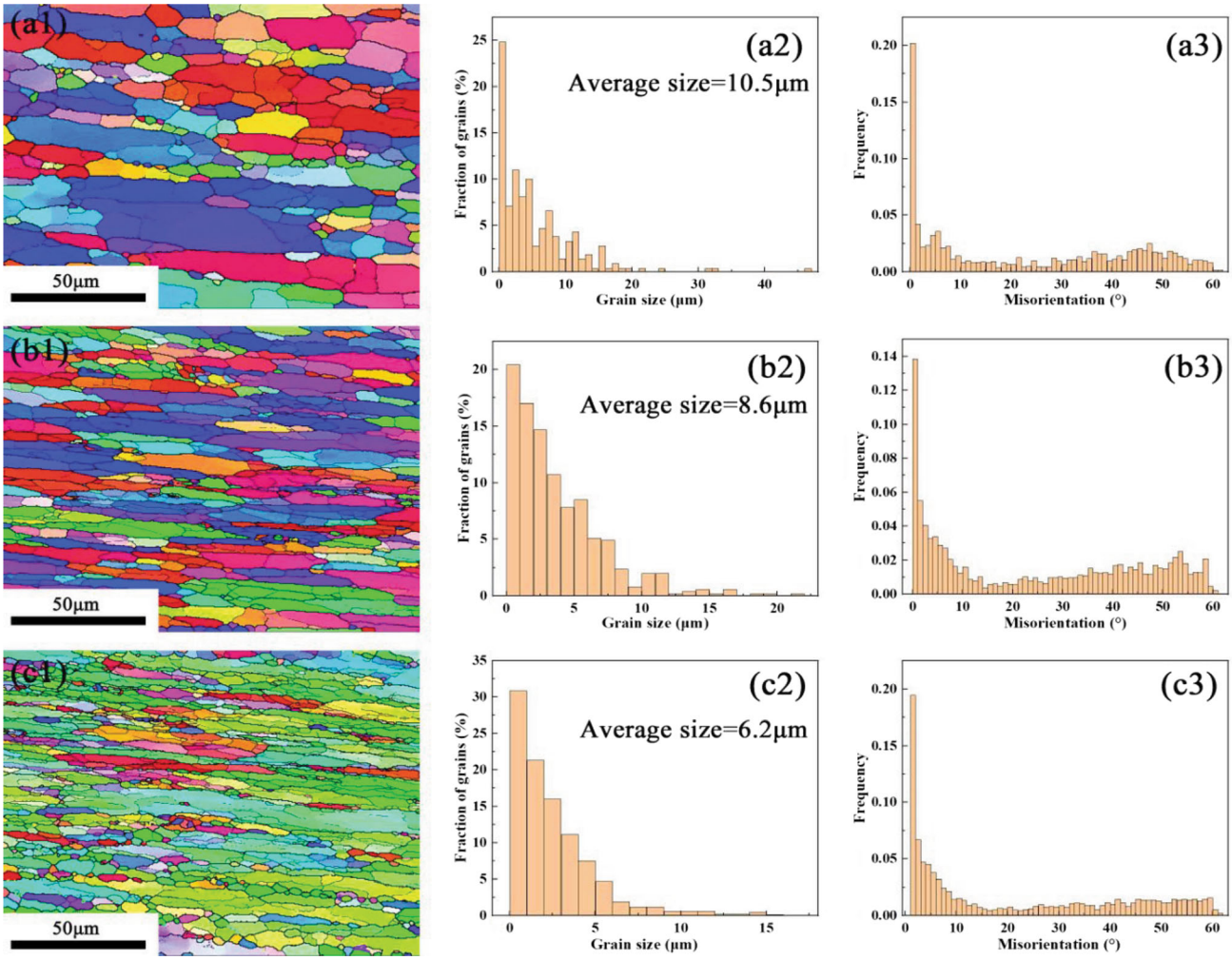

Fig. 7 EBSD IPF images, grain size and misorientation after hot compressed at different strain rates: (a1–a3) 0.01 s^{-1}; (b1–b3) 0.1 s^{-1}; (c1–c3) 1 s^{-1}

grains are formed (marked by the black arrow) at 400 °C, which are characterized by a DRX mechanism. Moreover, the irregular grains still exist in some local areas, indicating the main softening mechanism of DRX. After hot compression at 450 °C, the recrystallized grains (marked by the black arrows in Fig. 5c1) are formed due to the DRX. The average sizes of grains are refined to approximately 8.6 μm at this condition. The (110) ⟨001⟩, (111) ⟨110⟩ and (110) ⟨112⟩ are the main grain orientation at 350 °C/0.1 s^{-1}. The high density (110) ⟨112⟩ orientation disappear at 400 °C. As the compression temperature increases to 450 °C/0.1 s^{-1}, the (111) ⟨112⟩ and (112) ⟨111⟩ orientation are also formed except for (110) ⟨001⟩ orientation. In this condition, the relatively stronger ⟨111⟩ orientation plays a key role in developing the recrystallization grains.

As the compression temperature increases from 350 to 450 °C, the grain misorientation angle increases, as shown in Fig. 5(a3)–(c3). The number of sub-grains with low-angle grain boundaries is approximately 50%, which are mainly caused by the slip of dislocations. It implies that the high-angle grain boundaries (HAGBs, > 15°) are transformed from the low-angle grain boundaries (LAGBs, 2°-15°) with increasing compression temperature. Thus, the sub-grains with LAGBs are continuously transformed into the recrystallized grains with HAGBs due to the DRX. Figure 6 shows the degree of recrystallization, deformed and undeformed of the high Zn alloy after hot compressed at different compression temperatures with the strain rate of 0.1 s^{-1}. The "substructured" represents the undeformed microstructure. As the temperature increases from 350 to 450 °C, the degree of recrystallization increases from 27.7 to 60.8% (Fig. 6c). It indicates 119% increase in the degree of recrystallization. Thus, it concludes that the grain sizes, grain orientation and morphologies are highly affected by the studied compression temperature and strain rate.

Figure 7 and 8 show the EBSD images of the Al-Zn-Mg-Sc alloy with high Zn concentration after hot compressed at different strain rates. The grain orientation, grain size and misorientation distribution of the alloy at the temperature of 450 °C are presented in Fig. 7. The relative smaller grains accompanied by the LAGBs are formed inside the deformed grains, as shown in Fig. 7(c1), (c2). It can be found that the average sizes of grains are refined to approximately 6.1 μm at the condition of 450 °C/1 s^{-1}. This result implies that the recrystallized grain growth is suppressed at the high strain rate due to insufficient time of heat dissipation and microstructure softening. In addition, the driving force of DRX increases with decreasing strain rate, leading to the increases in the nucleation

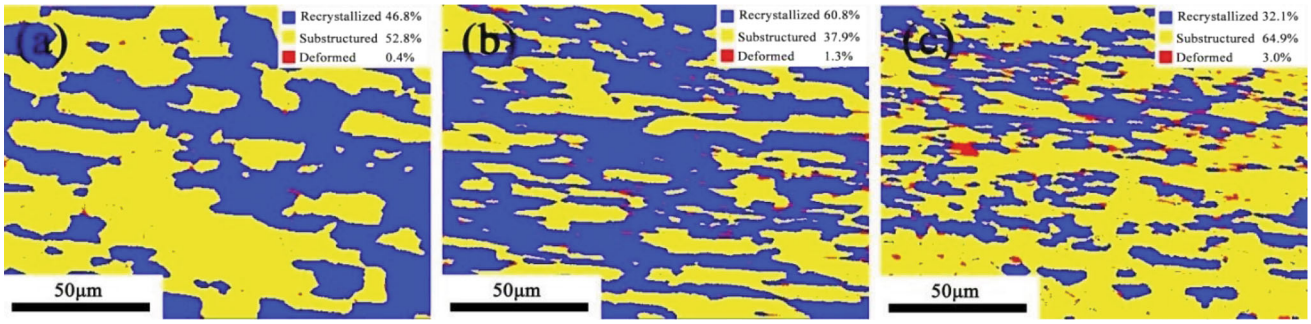

Fig. 8 The degree of recrystallization after hot compressed at different strain rates: (a) 0.01 s^{-1}; (b) 0.1 s^{-1}; (c) 1 s^{-1}

rate of the grains. At the strain rates of 0.01 and 0.1 s^{-1}, the grain size increases, and many HAGBs are generated, as presented in Fig. 7(a1), (a2), (b1), and (b2). The fine DRX grains are also produced along the initial grain boundaries. The dislocations continue to be absorbed by the sub-grains with LAGBs with decreasing strain rate. Meanwhile, the sub-grains are transformed into recrystallized grains, leading to the increases in the HAGBs and the large degree of accumulative strain in the original grains, as shown in Fig. 7(a3)–(c3). In addition, the main grain orientations are characterized by the (111) ⟨112⟩, (332) ⟨113⟩, (001) ⟨110⟩ and (112) ⟨111⟩ at 450 °C/0.01 s^{-1}. And the (111) ⟨110⟩ and (110) ⟨112⟩ orientations are dominate at 450 °C/1 s^{-1}, accompanied by many fine DRX grains with HAGBs. The change of grain orientation clarify that the recrystallized grains and microstructure softening behavior are also affected by the studied compression temperature and strain rate.

Figure 8 presents the degree of recrystallization, deformed, and undeformed of the Al-Zn-Mg-Sc alloy after hot compressed at different strain rates. The degree of recrystallization is approximately 32.1% at the condition of 450 °C/1 s^{-1}, and the undeformed grains reaches to 64.9%. The degree of recrystallization increases from 32.1% at 450 °C/1 s^{-1} to 60.8% at 450 °C/0.1 s^{-1}. It implies 89% increment in the degree of recrystallization and 41% decrement in the degree of undeformed grains, respectively. Unfortunately, the degree of recrystallization reduces to 46.8% in turn with decreasing strain rate continuous to 0.01 s^{-1}, as shown in Fig. 8(a). Since there is a sufficient time for the heat dissipation and DRX with decreasing strain rate, leading to the growth of recrystallized grains. Thus, the above results indicate that the DRV and DRX are the main softening mechanism of the Al-Zn-Mg-Sc alloy with high Zn concentration, which are closely associated with the studied compression temperature and strain rate.

4. Conclusions

(1) The true stress of the Al-Zn-Mg-Sc alloy with high Zn concentration increases rapidly with increasing accumulative strain, and finally reaches to a steady state. As the compression temperature decreases and strain rate increases, the peak value of true stress increases. The competing mechanism between work hardening and flow softening produce a crucial effect on the hot compression behavior of the high Zn alloy.

(2) The constitutive model with the activation energy of 102.657 kJ·mol^{-1} is established to describe the hot compression behavior of the Al-Zn-Mg-Sc alloy with high Zn concentration:

$$\dot{\varepsilon} = 6.17 \times 10^{6}[\sinh(0.01783\sigma)]^{5.6505}\exp[\frac{-102.657}{RT}]$$

(3) The softening mechanism is closely associated with compression temperature and strain rate. The DRV dominates under the low temperature and high strain rate. And the Al-Zn-Mg-Sc alloy is characterized by both the DRV and DRX at the high temperature and low strain rate. The relatively stronger ⟨111⟩ orientation plays an important role in developing the recrystallization grains. As the applied compression temperature increases and strain rate decreases, many sub-grains with LAGBs are transformed into recrystallized grains with HAGBs. The main softening mechanism is also transformed from DRV to DRX.

Acknowledgments

The authors are grateful for the financial support of the National Natural Science Foundation of China (No.51875383), the Natural Science Foundation of Guangxi (Nos. 2019GXNSFAA245051 and 2018GXNSFBA281056), and the Open Funding of Key Laboratory of New Processing Technology for Nonferrous Metal & Materials, Ministry of Education/Guangxi Key Laboratory of Optical and Electronic Materials and Devices (Nos. 20AA-8 and 20KF-7).

References

1. B.B. Straumal, B. Baretzky, A.A. Mazilkin, F. Phillipp, O.A. Kogtenkova, M.N. Volkov, and R.Z. Valiev, Formation of Nanograined Structure and Decomposition of Supersaturated Solid Solution During High Pressure Torsion of Al-Zn and Al-Mg Alloys, *Acta Mater.*, 2004, **52**, p 4469–4478
2. H.J. Jiang, C.Y. Liu, Z.Y. Ma, X. Zhang, L. Yu, M.Z. Ma, and R.P. Liu, Fabrication of Al-35Zn Alloys with Excellent Damping Capacity and Mechanical Properties, *J. Alloys Compd.*, 2017, **722**, p 138–144
3. A. Azarniya, A.K. Taheri, and K.K. Taheri, Recent Advances in Ageing of 7xxx Series Aluminum Alloys: A Physical Metallurgy Perspective, *J. Alloys Compd.*, 2019, **781**, p 945–983
4. H. Zhao, F.D. Geuser, A.K. Silva, A. Szczepaniak, B. Gault, D. Ponge, and D. Raabe, Segregation Assisted Grain Boundary Precipitation in a Model Al-Zn-Mg-Cu Alloy, *Acta Mater.*, 2018, **156**, p 318–329
5. M.A. Afifi, Y.C. Wang, P.H.R. Pereira, Y.W. Wang, S.K. Li, Y. Huang, and T.G. Langdon, Characterization of Precipitates in an Al-Zn-Mg

Alloy Processed by ECAP and Subsequent Annealing, *Mater. Sci. Eng. A*, 2018, **712**, p 146–156
6. Z.J. Ge, C.Y. Liu, H.F. Huang, and W. Cheng, Effects of mg Content and Heat Treatment on the Microstructure and Mechanical Properties of Rolled Al-Zn-Sc Alloy, *Mater. Charact.*, 2021, **173**, p 110932
7. H.J. Jiang, C.Y. Liu, Y. Chen, Z.X. Yang, H.F. Huang, L.L. Wei, Y.B. Li, and H.Q. Qi, Evaluation of Microstructure, Damping Capacity and Mechanical Properties of Al-35Zn and Al-35Zn-0.5Sc Alloys, *J. Alloys Compd.*, 2018, **739**, p 114–121
8. C.Y. Liu, X. Zhang, C.Q. Xia, Z.H. Feng, S.G. Liu, Z.G. Zhang, M.Z. Ma, and R.P. Liu, Effects of Sc Addition and Rolling on the Microstructure and Mechanical Properties of Al-35Zn Alloys, *Mater. Sci. Eng. A*, 2017, **703**, p 45–53
9. Y. Chen, C.Y. Liu, Z.Y. Ma, H.F. Huang, Y.H. Peng, and Y.F. Hou, Effect of Sc Addition on the Microstructure, Mechanical Properties, and Damping Capacity of Al-20Zn Alloy, *Mater. Charact.*, 2019, **157**, p 109892
10. C.Y. Liu, B. Qu, Z.Y. Ma, M.Z. Ma, and R.P. Liu, Recrystallization, Precipitation, and Resultant Mechanical Properties of Rolled Al-Zn Alloy After Aging, *Mater. Sci. Eng. A*, 2016, **657**, p 284–290
11. A. Alhamidi, K. Edalati, Z. Horita, S. Hirosawa, K. Matsuda, and D. Terada, Softening by Severe Plastic Deformation and Hardening by Annealing of Aluminum-Zinc Alloy: Significance of Elemental and Spinodal Decompositions, *Mater. Sci. Eng. A*, 2014, **610**, p 17–27
12. M. Ebrahimi, M.H. Shaeri, R. Naseri, and C. Gode, Equal Channel Angular Extrusion for Tube Configuration of Al-Zn-Mg-Cu Alloy, *Mater. Sci. Eng. A*, 2018, **731**, p 569–576
13. X.N. Meng, D.T. Zhang, W.W. Zhang, C. Qiu, G.G. Liang, and J.J. Chen, Microstructure and Mechanical Properties of a High-Zn Aluminum Alloy Prepared by Melt Spinning and Extrusion, *J. Alloys Compd.*, 2020, **819**, p 152990
14. J.H. Kim, J.H. Kim, J.T. Yeom, D.G. Lee, S.G. Lim, and N.K. Park, Effect of Scandium Content on the Hot Extrusion of Al-Zn-Mg-(Sc) Alloy, *J. Mater. Process. Technol.*, 2007, **187-188**, p 635–639
15. Q. Yang, Z. Deng, Z. Zhang, Q. Liu, Z. Jia, and G. Huang, Effects of Strain Rate on Flow Stress Behavior and Dynamic Recrystallization Mechanism of Al-Zn-Mg-Cu Aluminum Alloy During Hot Deformation, *Mater. Sci. Eng. A*, 2016, **662**, p 204–213
16. Q. Zang, H. Yu, Y.S. Lee, M.S. Kim, and H.W. Kim, Effects of Initial Microstructure on Hot Deformation Behavior of Al-7.9Zn-2.7Mg-2.0Cu (wt.%) Alloy, *Mater. Charact.*, 2019, **151**, p 404–413
17. C. Zhang, C. Wang, R. Guo, G. Zhao, L. Chen, W. Sun, and X. Wang, Investigation of Dynamic Recrystallization and Modeling of Microstructure Evolution of an Al-Mg-Si Aluminum Alloy During High-Temperature Deformation, *J. Alloys Compd.*, 2019, **773**, p 59–70
18. D.G. Cram, H.S. Zurob, Y.J.M. Brechet, and C.R. Hutchinson, Modelling Discontinuous Dynamic Recrystallization Using a Physically Based Model for Nucleation, *Acta Mater.*, 2009, **57**, p 5218–5228
19. S. Gourdet, and F. Montheillet, A Model of Continuous Dynamic Recrystallization, *Acta Mater.*, 2003, **51**, p 2685–2699
20. L.D. Pari, and W.Z. Misiolek, Theoretical Predictions and Experimental Verification Of Surface Grain Structure Evolution for AA6061 During Hot Rolling, *Acta Mater.*, 2008, **56**, p 6174–6185
21. K. Huang, and R.E. Loge, A Review of Dynamic Recrystallization Phenomena in Metallic Materials, *Mater. Des.*, 2016, **111**, p 548–574
22. G. Chen, L. Chen, G. Zhao, C. Zhang, and W. Cui, Microstructure Analysis of an Al-Zn-Mg Alloy During Porthole Die Extrusion Based on Modeling of Constitutive Equation and Dynamic Recrystallization, *J. Alloy Compd.*, 2017, **710**, p 80–91
23. B. Li, Q.L. Pan, and Z.M. Yin, Characterization of Hot Deformation Behavior of As-Homogenized Al-Cu-Li-Sc-Zr Alloy Using Processing Maps, *Mater. Sci. Eng. A*, 2014, **614**, p 199–206
24. Y.C. Lin, Y. Ding and M.S. Chen, A New Phenomenological Constitutive Model for Hot Tensile Deformation Behaviors of a Typical Al-Cu-Mg Alloy, *Mater. Des.*, 2013, **52**, p 118–127
25. H.J. McQueen, and N.D. Ryan, Constitutive Analysis in Hot Working, *Mater. Sci. Eng. A*, 2002, **322**, p 43–63
26. Y. Sun, L.K. Bao, and Y.H. Duan, Hot Compressive Deformation Behaviour and Constitutive Equations of Mg-Pb-Al-1B-0.4Sc Alloy, *Philos. Mag.*, 2021, **101**, p 2355–2376
27. M. Bambach, I. Sizova, J. Szyndler, J. Bennett, G. Hyatt, J. Cao, T. Papke, and M. Merklein, On the Hot Deformation Behavior of Ti-6Al-4V Made by Additive Manufacturing, *J. Mater. Process. Technol.*, 2021, **288**, 116840
28. H.R.R. Ashtiani, M.H. Parsa, and H. Bisadi, Constitutive Equations for Elevated Temperature Flow Behavior of Commercial Purity Aluminum, *Mater. Sci. Eng. A*, 2012, **545**, p 61–67
29. Y.H. Duan, P. Li, L.S. Ma, and R.Y. Li, Dynamic Recrystallization and Processing Map of Pb-30Mg-9Al-1B Alloy During Hot Compression, *Metall. Mater. Trans. A*, 2017, **48**, p 3419–3431
30. X.M. Qian, N. Parson, and X.G. Chen, Effects of Mn Addition and Related Mn-Containing Dispersoids on the Hot Deformation Behavior of 6082 Aluminum Alloys, *Mater. Sci. Eng. A*, 2019, **764**, 138253
31. W.Z. Bao, L.K. Bao, D. Liu, D.Y. Qu, Z.Z. Kong, M.J. Peng, and Y.H. Duan, Constitutive Equations, Processing Maps, and Microstructures of Pb-Mg-Al-B-0.4Y Alloy Under Hot Compression, *J. Mater. Eng. Perform.*, 2020, **29**(1), p 607–619
32. J.H. Zhao, Y.L. Deng, J.G. Tang, and J. Zhang, Influence of Strain Rate on Hot Deformation Behavior and Recrystallization Behavior Under Isothermal Compression of Al-Zn-Mg-Cu Alloy, *J. Alloys Compd.*, 2019, **809**, 151788
33. B. Li, Q.L. Pan, C.P. Chen, H.H. Wu, and Z.M. Yin, Effects of Solution Treatment on Microstructural and Mechanical Properties of Al-Zn-Mg Alloy by Microalloying with Sc and Zr, *J. Alloys Compd.*, 2016, **664**, p 553–564
34. J. Yan, Q.L. Pan, B. Li, Z.Q. Huang, Z.M. Liu, and Z.M. Yin, Research on the Hot Deformation Behavior of Al-6.2Zn-0.70Mg-0.3Mn-0.17Zr Alloy Using Processing Map, *J. Alloys Compd.*, 2015, **632**, p 549–557
35. F.C. Qin, H.P. Qi, and Y.T. Li, A Comparative Study of Constitutive Characteristics and Microstructure Evolution Between Uniaxial and Plane Strain Compression of an AA6061 Alloy, *J. Mater. Eng. Perform.*, 2019, **28**(6), p 3487–3497
36. F.C. Qin, H.P. Qi, Y.T. Li, C.Y. Liu, and H.Q. Qi, Deformation Behavior and Processing Maps of 42CrMo Alloy Casting Blank Subjected to Double-Pass Isothermal Compression, *J. Mater. Eng. Perform.*, 2021, **30**(5), p 3232–3242
37. R. Zhu, Q. Liu, J. Li, S. Xiang, Y. Chen, and X. Zhang, Dynamic Restoration Mechanism and Physically Based Constitutive Model of 2050 Al-Li Alloy During Hot Compression, *J. Alloys Compd.*, 2015, **650**, p 75–85
38. Q. Dai, Y. Deng, J. Tang, and Y. Wang, Deformation Characteristics and Strain-Compensated Constitutive Equation for AA5083 Aluminum Alloy Under Hot Compression, *Trans. Nonferrous Met. Soc. China*, 2019, **29**, p 2252–2261
39. J. He, J. Wen, X. Zhou, and Y. Liu, Hot Deformation Behavior and Processing Map of Cast 5052 Aluminum Alloy, *Procedia Manuf.*, 2019, **37**, p 2–7
40. J. Jiang, F. Jiang, H. Huang, M. Zhang, Z. Tang, and M. Tong, Hot Deformation Analysis and Microstructure Evolution of Al-Mg-Mn-Sc-Zr Alloy by Isothermal Compression, *J. Alloys Compd.*, 2020, **858**, 157655